Available online at www.sciencedirect.com
ScienceDirect
Journal of Hazardous Materials 140 (2007) 465–477
Journal of Hazardous Materials
www.elsevier.com/locate/jhazmat

Keys to modeling LNG spills on water

D.W. Hissong *

ExxonMobil Upstream Research Company, P.O. Box 2189, Houston, TX, USA

Available online 20 October 2006

Abstract

Although no LNG ship has experienced a loss of containment in over 40 years of shipping, it is important for risk management planning to understand the predicted consequences of a spill. A key parameter in assessing the impact of an LNG spill is the pool size. LNG spills onto water generally result in larger pools than land spills because they are unconfined. Modeling of LNG spills onto water is much more difficult than for land spills because the phenomena are more complex and the experimental basis is more limited.

The most prevalent practice in predicting pool sizes is to treat the release as instantaneous or constant-rate, and to calculate the pool size using an empirical evaporation or burn rate. The evaporation or burn rate is particularly difficult to estimate for LNG spills on water, because the available data are so limited, scattered, and difficult to extrapolate to the large releases of interest.

A more effective modeling of possible spills of LNG onto water calculates, rather than estimating, the evaporation or burn rate. The keys to this approach are to:

- Use rigorous multicomponent physical properties.
- Use a time-varying analysis of spill and evaporation.
- Use a material and energy balance approach.
- Estimate the heat transfer from water to LNG in a way that reflects the turbulence.

These keys are explained and demonstrated by predictions of a model that incorporates these features. The major challenges are describing the effects of the LNG–water turbulence and the heat transfer from the pool fire to the underlying LNG pool. The model includes a fundamentally based framework for these terms, and the current formulation is based on some of the largest tests to-date. The heat transfer coefficient between the water and LNG is obtained by applying a "turbulence factor" to the value from correlations for quiescent film and transition boiling. The turbulence factor is based on two of the largest unignited tests on water to-date. The heat transfer from the fire to the pool is based on the burning rate for the largest pool fire test on land to-date.

Keywords: LNG; Pool model; Vaporization; Pool fire

1. Introduction

With increasing quantities of liquefied natural gas (LNG) moving on world markets, operators of facilities and ships that handle LNG have engineering designs and procedures to ensure that their operations are safe. Although no LNG ship has experienced a loss of containment at port or at sea in over 40 years of shipping, it is important for risk management planning to understand the predicted consequences of a spill. An accidental release of LNG and subsequent vaporization and/or combustion involves very complex phenomena. To predict such effects, models with considerable simplifications are typically used, but it is important that the models capture the effects of the most important phenomena. The best models have as much theoretical basis as possible and are able to match experimental data. Unfortunately, the experiments to-date have some limitations relative to the situations for which predictions are desired. The tests have been relatively small-scale, and there is considerable uncertainty about the best way to scale key parameters to the release rates possible under certain scenarios. Most of the LNG pool fire tests have been on land, and the few fire tests on water show much different results. The reason for this difference is that a spill on water involves turbulent mixing of the LNG and water, which results in much greater heat transfer than for a spill on

* Tel.: +1 713 431 4517; fax: +1 713 431 6387.
E-mail address: doug.w.hissong@exxonmobil.com.

0304-3894/$ – see front matter © 2006 Elsevier B.V. All rights reserved.
doi:10.1016/j.jhazmat.2006.10.040

Nomenclature

A	pool area
Ar	Archimedes number
B	burning rate (mass)
c	heat capacity
D	pool diameter
f	interpolation function for transition boiling heat transfer coefficient
Fo	Fourier number $= \alpha t/\delta^2$
F_T	turbulence factor
f_1, f_2	functions for film boiling heat transfer coefficient
g	gravitational acceleration
g_c	unit conversion
h	heat transfer coefficient
H_D	height at which LNG is discharged
ΔH_V	heat of vaporization
k	thermal conductivity
K_A	attenuation constant for burning rate
K_S	spreading rate constant
L_c	critical length
M	mass
Nu	Nusselt number $= hD/k$
Pr	Prandtl number $= c\mu/k$
q	heat flux
Q	heat flow
R	pool radius
Re	Reynolds number $= Dv\rho/\mu$
S	spill rate (volumetric)
t	time
T	temperature
T_O	optical thickness of flame
v	velocity
V	volume of pool

Greek letters

α	thermal diffusivity $= k/\rho c$
δ	average pool thickness
μ	viscosity (absolute or dynamic)
ρ	density (mass)
σ	interfacial tension (vapor/liquid)

Subscripts

a	ambient air
D	at discharge point
F	film conditions
i	ith time step
w	water (as substrate)
L	liquid LNG
S	at water surface
V	LNG vapor

land. More tests have been conducted on unignited LNG spills on water, but most of these tests used idealized conditions. In all but one test series measures were taken to minimize the mixing of the LNG and water, which minimizes the important effect of turbulence. Because of the additional complexity of a burning pool, pool fires have been modeled in a less theoretically based manner than has been used for unignited pools.

2. Steps in consequence analysis

Analyzing the consequences of an LNG spill involves the following steps:

1. Predict the rate of release of LNG from the vessel versus time.
2. Predict the diameter of the liquid pool (whether unignited or ignited) versus time.
3. If the pool is unignited:
   - Predict the vaporization rate from the pool versus time.
   - Predict atmospheric dispersion of the vapor.
   - Estimate possible impacts of delayed ignition based on gas concentrations relative to the flammability limits of the gas when mixed with air.
4. If the pool is ignited:
   - Predict the size of the pool fire versus time and the thermal radiation at points of interest.
   - Estimate the impacts based on radiation levels and possible exposure duration.

Note that at every step it is important to include the variation with time. An "instantaneous release" scenario is an asymptotic limit that is unrealistic even for very large holes. A "constant release rate" scenario is the asymptotic limit for very small holes. The instantaneous and constant-rate assumptions can introduce considerable error into the predictions.

This paper focuses on predicting the pool diameter, because this is particularly challenging and current methods are lacking. For an ignited pool, the pool diameter defines the extent of flame engulfment and is a key parameter in predicting radiation levels outside the fire. Many radiation models, including the LNGFIRE3 model recommended for LNG pool fire radiation, do not predict the pool fire diameter but require it as an input for radiation predictions. For an unignited pool, the pool diameter controls the total vapor evolution rate and hence downwind gas concentrations predicted from it. This paper focuses on LNG pools on water, because this is particularly challenging and current methods have significant limitations.

3. Unignited spills

When LNG is spilled, some vapor is generated immediately. It is possible to form some aerosol, which is a suspension of liquid droplets so small that they will not settle out of the vapor/air mixture. The vapor and aerosol immediately contribute to the vapor cloud that forms. However, the fact that LNG is stored essentially as a saturated liquid means that little of it will flash

immediately or form an aerosol. By far most of the LNG will reach the surface below, either the ground or water, as liquid, forming a liquid pool that evaporates. Vapor evolved from the pool is the primary source for the vapor cloud.

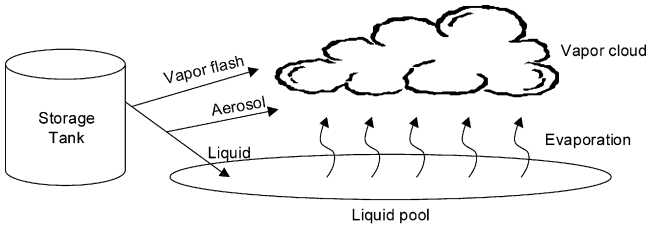

Formation of Liquid Pool and Vapor Cloud When LNG is Spilled

The liquid rate versus time from the release calculation is the input for the pool calculations.

Sometimes the area of the liquid pool is predicted by dividing the spill rate by an evaporation flux (kg/s m^2 or lb/s ft^2). However, the evaporation flux depends on so many variables that it is difficult to predict for a specific situation. It is much better to use the following approach.

The liquid portion of the LNG spreads out on the surface. For LNG, most of the literature suggests that this spreading is in the "gravity–inertia" regime where gravitational and inertial forces control. The pressure head provides the force to accelerate the LNG radially. By equating the gravity and inertial forces, one can derive the spreading relationship [1]. For a spill on water, the spreading relationship includes a relative density term reflecting the fact that the LNG layer displaces the water downward to some extent (i.e. partially "sinks into the water"):

$$\frac{\mathrm{d}R}{\mathrm{d}t} = K_S \sqrt{g\left(\frac{\rho_w - \rho_L}{\rho_w}\right)\delta} \tag{1}$$

where R is the pool radius (m, ft), t the time (s), K_S the spreading constant, g the acceleration due to gravity (m/s^2, ft/s^2), ρ_w the density of water (kg/m^3, lb/ft^3), ρ_L the density of LNG liquid (kg/m^3, lb/ft^3) and δ is the thickness of LNG layer (m, ft).

There is a theoretical value of 1.16 for the spreading constant K_S, but most experts agree that in order to match experimental data a higher value must be used. The most commonly suggested value is 1.41 $\left(\sqrt{2}\right)$ [1].

Following the gravity–inertia spreading regime, some liquids enter regimes in which friction (viscous) and surface tension forces control. Friction may be significant for some LNG spills, particularly on relatively rough water. If so, appropriate spreading equations can be used in the methodology.

To predict the pool diameter as a function of time, one must combine the spreading relationship with the evaporation rate, which is determined by an energy balance. The two relationships are solved simultaneously in a calculation that proceeds through a number of time steps. For each time step, the following calculations are done:

1. The pool radius is determined using the spreading relationship:

$$R_i = R_{i-1} + \left(\frac{\mathrm{d}R}{\mathrm{d}t}\right)(t_i - t_{i-1}) \tag{2}$$

where R_i is the pool radius at time t_i (m, ft), R_{i-1} the pool radius at time t_{i-1} (m, ft) and t_i, t_{i-1} is the times at end and beginning of current time step (s).

2. The mass of LNG remaining is determined by a mass balance:

$$M_i = M_{i-1} + M_{rel} - M_{evap} \tag{3}$$

where M_i is the mass of LNG in pool at time t_i (kg, lb), M_{i-1} the mass of LNG in pool at time t_{i-1} (kg, lb), M_{rel} the mass of LNG released between times t_{i-1} and t_i and M_{evap} is the mass of LNG evaporated between times t_{i-1} and t_i.

3. The mass evaporated is determined from the heat of vaporization and an energy balance:

$$M_{evap} = \frac{Q(t_i - t_{i-1})}{\Delta H_V} \tag{4}$$

$$Q = Q_{sub} + Q_{air} + Q_{rad} \tag{5}$$

where ΔH_V is the heat of vaporization of LNG (J/kg, Btu/lb), Q the total heat flow (W, Btu/s), Q_{sub} the heat flow from substrate to LNG (W, Btu/s), Q_{air} is the heat flow from air above LNG pool (W, Btu/s) and Q_{rad} radiative heat flow from above LNG pool (W, Btu/s).

4. The volume of LNG in the pool (V_i) is calculated from the mass and density (ρ_L):

$$V_i = \frac{M_i}{\rho_L} \tag{6}$$

5. The average pool thickness (δ_i) is calculated from the volume and area:

$$\delta_i = \frac{V_i}{\pi R_i^2} \tag{7}$$

The spreading relationship (Eqs. (1) and (2)) is used until the thickness reaches the minimum stable pool thickness. After that, the thickness is fixed at the minimum value and the pool radius is calculated from the pool volume. The minimum stable pool thickness depends on the surface on which the LNG is spilled. For spills on water, it depends on the extent or absence of waves, which in turn depends on wind. In two tests conducted by Esso on open water, the minimum stable thicknesses were about 6.7 and 4.4 mm [2].

A liquid spill model developed by Exxon [3] uses essentially this methodology. It uses radius versus time equations from the same source (Ref. [1]), and includes prediction of release rates from a tank (including vaporization and aerosol formation). Some details of the energy balance terms differ from those used in this work. This model, originally called LSM90, was incorporated into Shell's HGSYSTEM [4] as the model LPOOL.

Appendix A presents the correlations used for the heat flow terms in Eq. (5).

In evaluating the energy balance terms and the heat of vaporization, it is important to use physical properties that reflect the

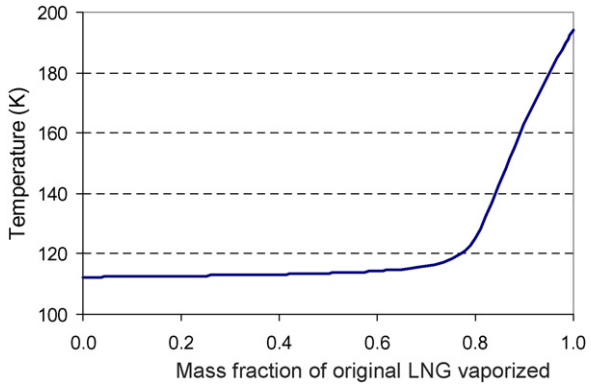

Fig. 1. Variation of saturation temperature with fraction vaporized.

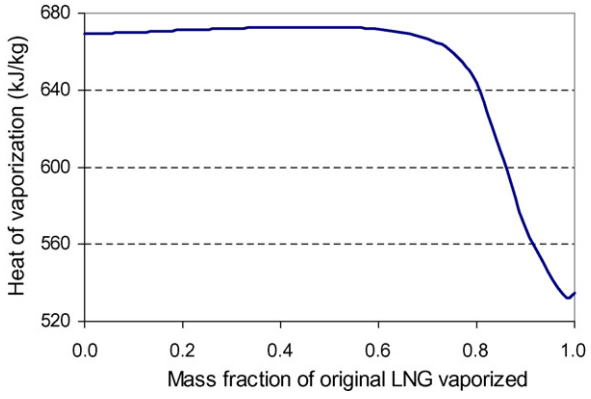

Fig. 2. Variation of heat of vaporization with fraction vaporized.

actual LNG composition and the change in composition due to vaporization. Figs. 1 and 2 show how the saturation temperature and heat of vaporization, respectively, of the liquid remaining in the pool vary as the original LNG is vaporized. As the pool evaporates, the temperature of the remaining liquid increases and hence the temperature difference driving the heat transfer decreases. Most of the change occurs after the LNG is about 2/3 evaporated. The heat of vaporization (on a mass basis) of the remaining liquid increases through a weak maximum, then decreases. All the physical properties change. As an illustration, the following table shows selected properties at 2% and 95% vaporization of a typical LNG (Table 1 shows the composition of the LNG used in this work):

Table 1
Composition of typical LNG

Component	Mole (%)
Nitrogen	0.1
Methane	92.0
Ethane	3.9
Propane	2.7
Isobutane	0.69
n-Butane	0.60
n-Pentane	0.01
Total	100

Fraction vapor (mass)	Temperature (K)	Liquid			Vapor density (kg/m^3)	Heat of vaporization (kJ/kg)
		Molecular weight (kg/kg mol)	Density (kg/m^3)	Heat capacity (J/kg K)		
0.02	112	17.9	458	3116	1.822	669
0.95	180	50.4	662	1775	1.187	544

Change in physical properties as original LNG is vaporized.

Such changes have a significant effect on vaporization predictions.

Studies have shown that the vaporization of LNG is quite different from that of pure methane and that the vaporization rate decreases considerably in the later stages of vaporization. Conrado and Vesovik [5] says that treating LNG as methane will lead to underestimating the vaporization time by 10–15% and that neglecting the liquid composition change will lead to about a 20% underestimate. Boe [6] points out that mixtures have higher heat transfer coefficients than pure components, due to localized effects of the preferential evaporation. His experiments showed early time evaporation rates for an LNG-like mixture about 10 times higher than for pure methane.

This methodology for spills on water has been implemented in an Excel spreadsheet. Release rates as a function of time are determined using the Bernoulli equation, accounting for the shape of the tank. The spreadsheet uses these rates in a series of time steps as discussed above. The required physical properties are determined using the HYSYS process simulator, using the Peng–Robinson Volume-Translated equation of state. The properties are tabulated as a function of the fraction of the LNG vaporized. At each time step, the fraction vaporized is calculated by dividing the total mass vaporized by the total mass spilled. This fraction is used to interpolate on the property tables.

4. Effect of LNG–water turbulence

LNG spills on water differ from those on land in that:

1. They are generally unconfined, or atleast less confined.
2. The heat transfer rate is much greater and does not decrease with time because the water recirculates, providing a more constant temperature difference.

For a spill on water, the heat flow from the substrate to the LNG can be expressed with a convection equation:

$$Q_{\text{sub}} = h_{\text{w}} \pi R_i^2 (T_{\text{w}} - T_{\text{L}}) \quad (8)$$

where Q_{sub} is the heat flow from substrate to LNG (W, Btu/s), h_{w} the heat transfer coefficient between water and LNG (W/m^2 K, Btu/s ft^2 F), R_i the radius of pool at time step i (m^2, ft^2), T_{w} the temperature of water (K, F) and T_{L} is the temperature of LNG pool (K, F).

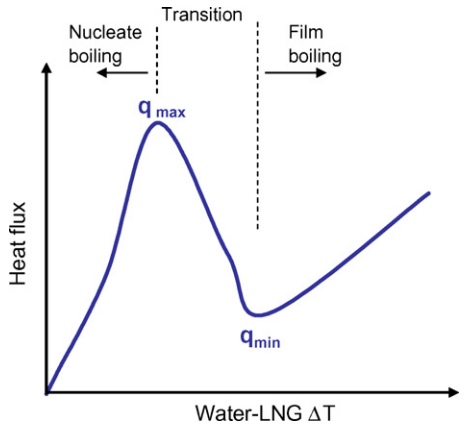

Fig. 3. Typical boiling heat flux curve.

Fig. 3 shows the general relationship between heat flux and temperature difference. At high temperature differences, the boiling is termed "film boiling" because a film of LNG vapor exists between the water and the liquid LNG. At lower temperature differences, the film breaks up and the boiling moves into the transition region between film boiling and nucleate boiling. This transition results in a higher heat transfer coefficient.

Appendix A presents the correlations used in this work for the minimum temperature difference required for film boiling and for the heat transfer coefficients in the film boiling and transition regions. The correlations indicate that for the LNG composition shown in Table 1 the boiling enters the transition region when ~69% (by mass) of the LNG has evaporated. For the LNG compositions used in some of the field tests simulated here, the transition begins when ~84% of the LNG has evaporated. The temperature difference between the water and LNG goes from ~190 to 150 K (~340–270 °F) as evaporation proceeds. The minimum temperature difference required for film boiling (corresponding to q_{min} in Fig. 3) goes from ~140 to 280 K (~250–510 °F). The maximum temperature difference for nucleate boiling (corresponding to q_{max} in Fig. 3) is only 3–4 K (5–8 °F). This means that the boiling moves only slightly into the transition region before evaporation is complete. The change in boiling regime causes an increase in the heat transfer coefficient near the end of the evaporation.

The correlations predict a heat transfer coefficient between the water and LNG of ~150 W/m^2 K (27 Btu/h ft^2 F), which with the temperature difference, corresponds to a heat flux of ~28 kW/m^2. The practice to-date in spill evaporation models has been to use such values. The problem is that the standard correlations for boiling heat transfer are for quiescent conditions. They apply if the LNG is placed onto the water with minimal disruption of the water surface and minimal mixing of the LNG with the water. However, in realistic spills the LNG and water mix in a manner that generates considerable turbulence. The LNG falls into the water at a velocity of ~15 m/s (50 ft/s). A correlation based on experiments [7] indicates that the jet of LNG will go at least 13 m (43 ft) underwater. The two liquids will swirl around, mixing extensively, and the rapid vaporization will further agitate the mixing zone. This greatly increases the heat transfer between the phases and hence the evaporation rate. The literature includes ample experimental evidence that turbulence between spilled LNG and water can greatly increase the vaporization rate. Some examples follow:

- The Bureau of Mines [8] conducted some small-scale tests in which a thin (32-mil) aluminum sheet was placed on the water surface. LNG was poured onto the aluminum surface. The presence of the metal sheet led to "a much lower evaporation rate than from the water surface and a much faster decline of this evaporation rate with time". Average values of the evaporation rate and derived heat flux for the experiments were as follows:

Metal sheet?	Evaporation rate (kg/s m^2)	Heat flux (kW/m^2)
No	0.155	89.6
Yes	0.072	41.8

Effect on LNG evaporation of metal sheet on water surface.

- The average evaporation rates and heat fluxes reported in tests show a dependence on the manner in which the LNG was delivered to the water surface:

Tests	Delivery method	Evaporation rate (kg/s m^2)	Heat flux (kW/m^2)
Esso (1972) [2]	Sprayed upward, falling onto water	0.194	131
BuMines (1970) [9]	Dumped from ~2 ft above water	0.177	103
Maplin Sands (1980) [10]	Horizontal distribution plate at water surface	0.085	
Quiescent film boiling		0.042	28

Effect on evaporation of method of delivery of LNG to water surface.

The evaporation rate and heat flux increase as the delivery involves more mixing of the LNG with the water. For comparison, the bottom line in the table shows typical values for quiescent film boiling (using the standard correlations presented in Appendix A).

- In one of the Maplin Sands tests, the LNG was released below the water surface. The behavior was much different from the other tests in which the LNG was released above the water surface. Shell reported that for the subsurface release "so much heat was absorbed at the source that the cloud rapidly became buoyant and lifted off from the surface [10]".
- In two tests by the Bureau of Mines [7], LNG was suddenly released 3–4.5 m (10–15 ft) below the water surface. The LNG vaporized completely before reaching the water surface, such that no liquid pool was observed.
- Burning rates for pool fires on water are much higher than for pool fires on land, and they increase with increasing spill rate (as will be discussed).

The procedure used in this work to account for the effect of turbulence between the spilled LNG and the water is to develop a correlation for the turbulence factor, which is the ratio of the actual heat transfer coefficient between the water and LNG to

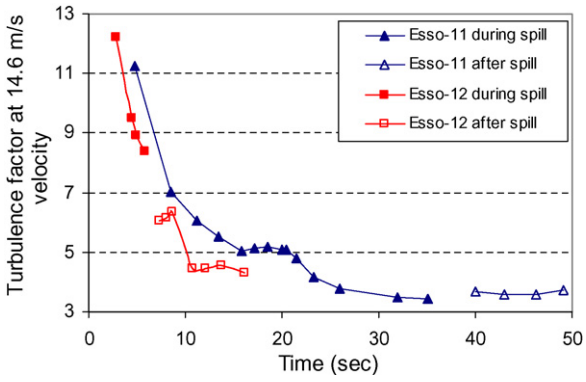

Fig. 4. Turbulence factors calculated for Esso tests.

the value based on standard (quiescent) boiling:

$$F_T = \frac{h_w}{h_q} \tag{9}$$

where F_T is the turbulence factor, h_w the heat transfer coefficient between water and LNG (W/m^2 K, Btu/s ft^2 F) and h_q is the quiescent heat transfer coefficient from correlations (W/m^2 K, Btu/s ft^2 F).

Heat transfer coefficients were derived from two spill tests on water in which pool diameter and evaporation rate were reported as functions of time. These tests were conducted by Esso in a joint industry project for the American Gas Association [2]. The calculation steps were as follows:

1. From the diameter and evaporation rate, calculate the evaporation flux.
2. From the evaporation flux and the heat of vaporization, calculate the total heat flux to the LNG.
3. Subtract the heat flux from the air and the radiation flux to get the heat flux from the water to the LNG.
4. From the temperature difference between the water and LNG, calculate the heat transfer coefficient.

These tests were simulated with the above procedure so the necessary physical properties and the film boiling heat transfer coefficient could be determined for each time step. Fig. 4 shows the turbulence factors for these tests. In Test 11 LNG was spilled for 35 s, and in Test 12 it was spilled for 6.2 s. During the spill, the turbulence factor, which is based on the total pool area, decreases with time because the highly turbulent region near the spill becomes a smaller fraction of the total pool. Note that the heat transfer early in a spill can be an order of magnitude greater than for quiescent boiling, and that even after the spill stops it remains three to four times greater than for quiescent boiling. These tests were conducted in open water in the Gulf of Mexico.

Heat transfer coefficients generally depend on the fluid velocity. For quantifying the extent of turbulence between the water and LNG, the relevant velocity is the velocity of the LNG as it hits the water surface. This can be calculated from the velocity at the release point and the distance of free-fall to the water surface:

$$v_S = \sqrt{v_D^2 + 2gH_D} \tag{10}$$

where v_S is the LNG velocity at water surface (m/s, ft/s), v_D the LNG velocity at discharge point (m/s, ft/s) and H_D is the height of discharge point above water surface (m, ft).

The velocity at the discharge point (v_D) will generally decrease somewhat with time, and can be calculated from the release rate, LNG density, and release area.

The velocity v_S was ~15 m/s in Test 11 and ~11 m/s in Test 12. The velocity for Test 11 is similar to the initial velocity for releases from typical spherical or membrane tanks on LNG ships. At such velocities, the heat transfer is dominated by forced convection. Predictions with a standard correlation for forced convection can be used to determine the effect of velocity on heat transfer coefficients. Such an analysis leads to the following relationship for adjusting the turbulence factor (at any time) for the LNG spill velocity (see Appendix A):

$$F_T = (F_T)_0 \left(\frac{v_S}{v_0} \right)^n \tag{11}$$

where $(F_T)_0$ is the turbulence factor at reference spill velocity, v_S the LNG velocity at water surface (m/s, ft/s), v_0 the reference LNG velocity at water surface (m/s, ft/s) and n is the velocity exponent (depends on release hole size).

The turbulence factors during the spill shown in Fig. 4 have been adjusted to a velocity of 14.6 m/s.

The turbulence factor accounts for many complex phenomena including increased interfacial area between the LNG (liquid and vapor) and water and the relative motion between the LNG and water.

The decrease in the turbulence factor with time due to the spreading of the pool can be correlated in terms of the Fourier number, which is a dimensionless time used in heat transfer (primarily conduction):

$$Fo = \frac{\alpha t}{\delta^2} \tag{12}$$

where Fo is the Fourier number, α the thermal diffusivity of liquid LNG (m^2/s, ft^2/s) = $k/\rho c$, k the thermal conductivity of liquid LNG (W/m K, Btu/s ft F), ρ the density of liquid LNG (kg/m^3, lb/ft^3), c the heat capacity of liquid LNG (J/kg K, Btu/lb F), t the time (s) and δ is the average pool thickness (m, ft).

The relationship based on Esso Tests 11 and 12 is:

$$(F_T)_0 = 10.0(Fo \times 10^3)^{-0.207} \tag{13}$$

where $(F_T)_0$ is the turbulence factor at the reference LNG velocity of 15 m/s. This correlation is shown in Fig. 5. This relationship should only be considered a first pass that can be improved when more data become available.

Beyond the effect of velocity (Eq. (11)), it is reasonable to expect that the turbulence factor will be affected by the scale of the LNG release, probably best expressed in terms of the

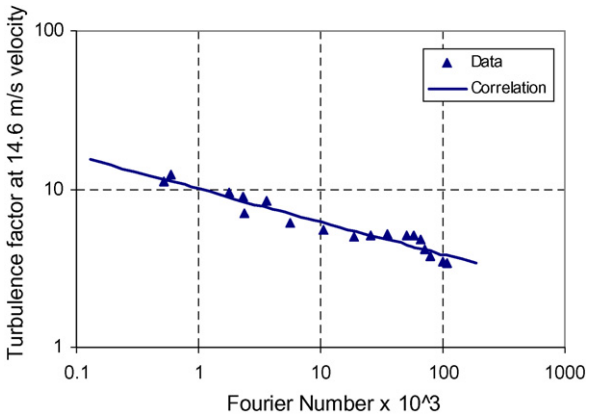

Fig. 5. Correlation of turbulence factors with Fourier number.

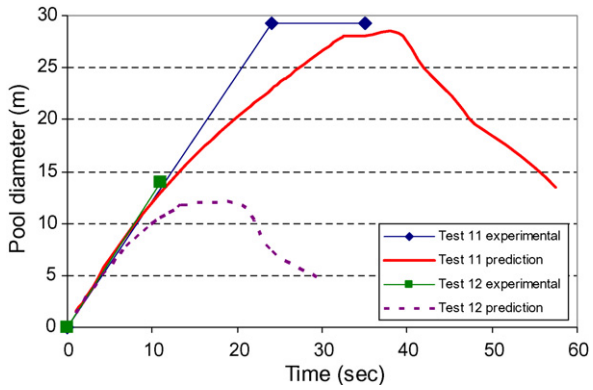

Fig. 6. Predicted pool diameters for Esso tests.

volumetric release rate. One possible expression is a power law:

$$F_T = (F_T)_0 \left(\frac{S_S}{S_0}\right)^m \quad (14)$$

where $(F_T)_0$ is the turbulence factor at reference spill rate, S_S the LNG volumetric spill rate (m^3/s, ft^3/s), S_0 the reference LNG spill rate (m^3/s, ft^3/s) and m is the spill rate exponent.

Unfortunately, there is very little basis to define the exponent at this time. The spill rates for Esso Tests 11 and 12 were 0.292 and 0.150 m^3/s (10.3 and 5.28 ft^3/s), respectively. The turbulence factors shown in Fig. 4 suggest an exponent m of about 0.2. This value has been used here, although this is clearly a topic warranting further study.

The above correlation and adjustment factors provide the turbulence factor while the LNG is being spilled. After the spill stops one should use a constant turbulence factor that depends on the wind and waves. For the open water conditions of Esso Tests 11 and 12, this factor was 3–4. When predicting the maximum pool diameter for possible real spills, this does not come into play because the maximum diameter is reached relatively quickly, before the spill stops.

The simulation procedure requires the minimum stable film thickness beyond which the pool breaks up. As mentioned above, for a spill on water this depends on the extent or absence of waves, which in turn depends on the wind. In two of the Esso tests, which were conducted on open water, the wind speed was 8.1–8.3 m/s (18–18.5 MPH) and the reported final film thicknesses were 4.4 and 6.7 mm (0.17 and 0.26 in.). Similar values would be expected for many water conditions. In most other tests the wind speed was lower, the body of water was smaller, and the water presumably smoother.

Fig. 6 shows the predicted pool diameter versus time for the two Esso tests, which are compared with the reported values. For Test 11, the predicted diameter reaches a maximum around the time when the release ended (35 s), whereas for Test 12 the release was so short (6 s) that the maximum diameter occurs some time after the release stopped. A single value of diameter was reported for a portion of the test during which it appeared relatively constant (near the end of the release). For Test 11, the average evaporation flux was also reported for the same period. The following table compares experimental values of key results with the model predictions:

	Maximum pool diameter (m)		Average evaporation flux for 24–35 s (kg/s m^2)	
	Experimental	Predicted	Experimental	Predicted
Test 11	29	14	0.19	0.21
Test 12	28	12		

Comparison of model predictions with experiments for unignited pools.

5. Pool fires on land

Since ignited spills (i.e. pool fires) are sufficiently more complex than unignited spills, the dominant approach to-date has been to use empirical "burning rates" instead of doing the kind of heat transfer analysis described above for unignited spills. The burning rate is the rate at which mass burns per unit time per unit of pool area, expressed in kg/s m^2 or lb/s ft^2. Some experimentalists report the "regression rate", which is the burning rate divided by the LNG density. It has units of velocity (m/s or ft/s) and can be visualized as the rate at which the top of a layer of LNG moves downward as the LNG burns.

A burning rate is a mass flux, which should be directly related to the total heat flux to the LNG pool. It includes the effects of several heat transfer mechanisms and many variables. For extrapolation to conditions much different from available tests, it is better to separate the heat transfer mechanisms and use more fundamental parameters. However, existing correlations for burning rates can be used in doing this.

Extending the heat transfer analysis from unignited pools to pool fires requires replacing the solar radiation term with the radiation downward from the fire to the pool.

The effect of pool diameter on burning rate is normally expressed by:

$$B = B_{max}[1 - \exp(-K_A D)] \quad (15)$$

where B is the burning rate for pool fire of diameter D (kg/s m^2, lb/s ft^2), B_{max} the maximum burning rate for large fires (kg/s m^2, lb/s ft^2), K_A the attenuation coefficient (1/m, 1/ft) and D is the pool diameter (m, ft).

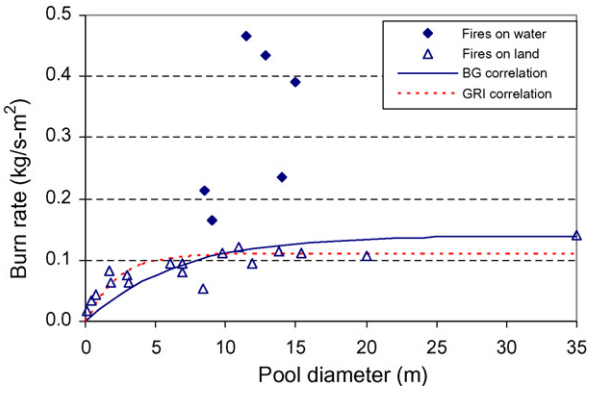

Fig. 7. Burning rates for LNG pool fires.

The explanation for this dependence is as follows [11]. Vaporization from the pool surface is due predominantly to radiation from the fire. As pool diameter increases the pool reaches a size at which it becomes "optically thick" such that further increase in diameter does not result in further increase in emitted radiation to the pool. In other words, there is a diameter at which radiative feedback to the pool surface reaches a maximum. The pool diameter at which this occurs (reflected in the attenuation coefficient) depends on the fuel.

Another way to look at this effect is that vapor evolved near the center of the pool fire does not have access to adequate air for it to burn until it reaches the top of the flames, so there is little radiation to the pool in the center of the pool. The fire burns around the edge of the pool (and the top of the flame), where the vapor and air can mix to form a flammable mixture.

The following correlations have been developed for pool fires on land:

Source	Software	Fluid	Correlation	D for maximum B
GRI [12]	LNGFIRE	LNG	$B = 0.11$ $[1 - \exp(-0.46D)]$	10 m
British Gas [13]	FIRE2	LNG, ethane	$B = 0.14$ $[1 - \exp(-0.156D)]$	30 m

Burning rate correlations for fires on land.

where B is in kg/s m^2 and D in m. The right-hand column gives the pool diameter for which the burning rate is 99% of the asymptotic maximum value.

Fig. 7 shows the two correlations and burning rate data from the LNGFIRE manual [12] for LNG pool fires on land (open points). It is not clear which correlation fits the data better, but the British Gas correlation is probably better for larger fires, since it matches the largest test to-date, the 35-m diameter Montoir test.

The following methodology can be used to predict pool fire sizes using the energy balance approach instead of empirical burning rates. Of course, the burning rate correlation is still used to capture the data from the experiments.

For a pool fire on land, heat transfer to the pool is dominated by radiation from the fire. Hence, the burning rate is directly related to the radiation flux to the pool. The burning rate reported for the Montoir test was 0.14 kg/s m^2 (reflected by the constant of 0.14 in the British Gas correlation above). Multiplying this value by the heat of vaporization of LNG gives a heat flux of 95 kW/m^2. Thus, the British Gas correlation for burning rate implies that radiation flux to the pool is:

$$q_{\text{rad}} = q_{\max}[1 - \exp(-0.156D)] \tag{16}$$

where q_{rad} is the heat flux to pool for pool fire of diameter D (kW/m^2), $q_{\max}$ the maximum heat flux to pool for large fires = 95 kW/m^2 and D is the pool diameter (m).

Taking the optical thickness as the pool radius when the burning rate is 99% of the asymptotic maximum value, the British Gas correlation implies that the optical thickness is:

$$T_{\text{O}} = \frac{1}{2}\left[\frac{-\ln(1-0.99)}{k_{\text{a}}}\right] = \frac{1}{2}\left[\frac{-\ln(0.01)}{0.156}\right] = 15\,\text{m} \tag{17}$$

When the pool radius exceeds T_{O}, a layer about 15 m thick is burning around the outside of the fire, surrounding a core where the vapor does not burn close to the pool surface because of a lack of air. The area of the outer zone, which receives the heat flux $q_{\max}$, is:

$$A_{\text{out}} = \pi(R_i^2 - T_{\text{O}}^2) \tag{18}$$

and the area of the inner zone is:

$$A_{\text{ins}} = \pi T_{\text{O}}^2 \tag{19}$$

There is debate about the extent to which the heat flux in the central portion of a pool fire is less than that around the edges. In this work, the heat flux to the pool in the inner zone is assumed to be half of $q_{\max}$, or 47.5 kW/m^2. The total radiation to the pool is the sum of the contributions from the two zones. This is clearly another area that warrants further study. Perhaps surprisingly, predicted pool fire sizes are less sensitive to estimates of heat transfer from the fire than to estimates of heat transfer from the water, since the latter is larger (with a proper accounting for LNG–water turbulence).

6. Pool fires on water

Fig. 7 also includes burning rate data for the only pool fire tests on water (solid points), the series conducted at China Lake. (The Maplin Sands tests were ignited at the end of the tests, illustrating flash fires but not providing pool fire data.) The burning rates for the fires on water are much higher because of turbulence between the LNG and water. Fig. 8 shows that the burning rates for the fires on water increase with increasing spill rate. This supports including the spill rate in the correlation for turbulence factors.

The burning rates for the tests on water were up to four times the values predicted for land fires. These burning rate ratios may be regarded as another estimate of the turbulence factor. However, in the China Lake series a spill plate at the water surface greatly reduced the LNG–water mixing and turbulence. The factor of four observed here agrees with the turbulence factor in Esso Tests 11 and 12 after the release stopped, which resulted in a more quiescent pool. Values from

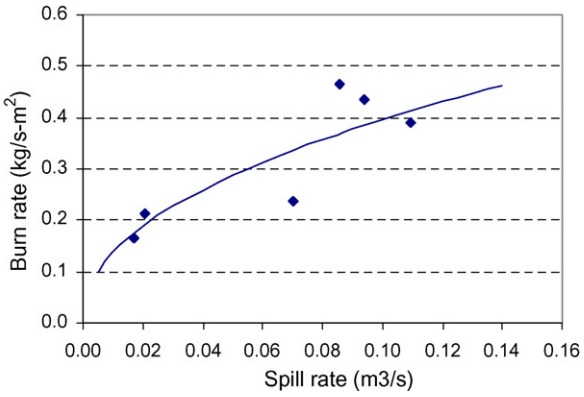

Fig. 8. Effect of spill rate on burning rates for LNG pool fires on water.

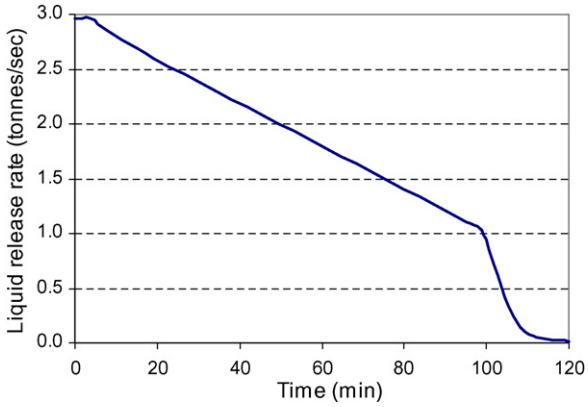

Fig. 9. Spill rate vs. time for 0.75-m hole at waterline.

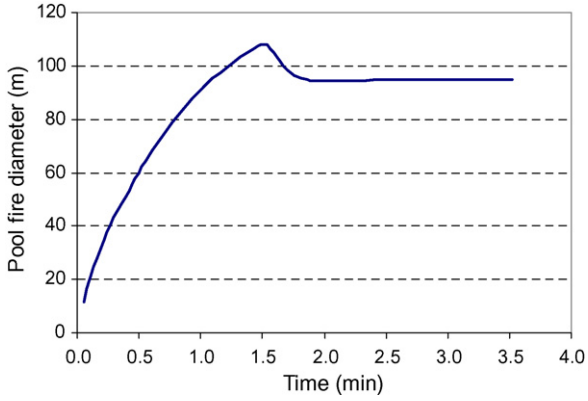

Fig. 10. Pool fire diameter for 0.75-m hole at waterline.

ignited tests do not serve as well for extrapolation as do the values based on the unignited tests. The effect of turbulence is better discerned in unignited tests where it is the dominant effect, i.e. where it is not complicated by the effects of a fire.

Some literature [14] suggests that the burning rate on water is 2.5 times that on land. This ratio would appear to be too low for large spills and particularly for realistic spills in which the LNG and water will mix extensively (as opposed to tests using a spill plate).

The burning rate correlation in the previous section is based on data for pool fires on land. For fires on water, even though the burning rates are higher one would expect the effect of the poor combustion near the center of the pool to be similar to that for fires on land. Those involved in the China Lake tests referred to "unburned fuel in the center of the fire column" [15]. Using land-fire data for the cooler-fire-center effect separates this effect from the effect of LNG–water turbulence.

The energy balance approach for predicting pool diameter can be applied to pool fires on water by using:

- The correlation for heat transfer coefficients between water and LNG based on unignited pools.
- The methodology for heat transfer from the fire to the pool based on pool fires on land.

In this way the two effects are kept separate and each is evaluated from the type of tests in which it is most discernable.

For pool fires on water, the heat transfer rate from the water to the pool, including the effect of turbulence, is greater than the heat transfer rate from the fire to the pool.

Predictions were made for two of the China Lake tests. Pool diameters were reported without reference to timing. These tests used a spill plate. In the simulations, no change was made to the turbulence factor correlation used during the spill, but the turbulence factor after the spill was reduced to account for the calmer water (a factor of 2 was used). The maximum pool diameters were:

	China Lake Test 4	China Lake Test 6
LNG spilled	4.2 m^3 in 248 s	5.7 m^3 in 52 s
Experimental fire diameter	9 m (29 ft)	15 m (49 ft)
Predicted fire diameter	7.9 m (26 ft)	21 m (68 ft)

Comparison of model predictions with experiments for ignited pools.

7. Predictions for a large spill

As an example of predictions for a large spill, Figs. 9–12 show the predictions for a hypothetical 0.75-m diameter hole in a 40,000 m^3 membrane ship tank. This hole diameter was selected on the basis of a recent study [14] as illustrative of the methodology only. There are no recognized guidelines or industry experience that substantiates likely or unlikely hole sizes for ships. The hole is just above the waterline, so that the LNG drains down to the waterline. About 2/3 of the LNG in the tank is above the waterline and hence released. Fig. 9 shows the spill rate as a function of time. The level of the LNG reaches the top of the hole in ∼100 min, and hence the rate decreases more rapidly after that.

The spill is assumed to be immediately ignited, e.g. by the event causing the hole. Fig. 10 shows that the pool fire reaches a maximum diameter of ∼108 m in ∼1.5 min.

At that point the pool area is such that the total LNG burning rate equals the release rate. As the release rate slowly decreases, the pool diameter slowly decreases. Fig. 11 shows the spill and evaporation rates. The evaporation rate exceeds the spill rate after ~0.8 min, then decreases after the maximum diameter is reached. Fig. 12 shows the mass of liquid in the pool, which goes through a maximum around the time when the spill and evaporation rates cross. The pool fire may last nearly as long as LNG liquid is being released from the tank, but the size of the fire will decrease as the release rate decreases. At some point, the fire will break up and go out, depending on the wind and waves. Vapor may continue to burn at the release point as the rest of the LNG in the tank vaporizes.

The following are results of some sensitivity cases analyzed:

Parameter changed	Time to maximum diameter (min)	Maximum pool diameter (m)
Base case	1.48	108
Constant properties	1.59	116
Properties of pure methane	1.21	94
Spill rate exponent $m = 0.05$ (vs. 0.2)	1.92	133
Minimum thickness = 3 mm (vs. 6 mm)	1.86	115
Unignited	1.90	126

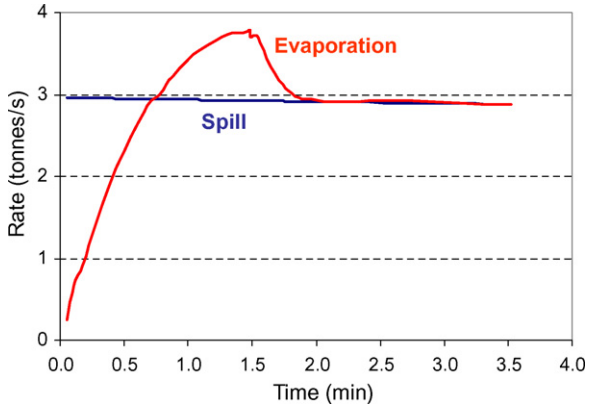

Fig. 11. Spill rate and evaporation rate for 0.75-m hole.

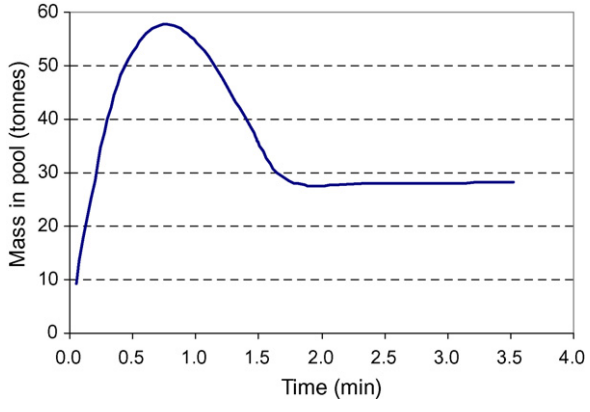

Fig. 12. Mass of liquid LNG in pool for 0.75-m diameter hole.

The last case shows the effect of heat transfer from the fire. Of course, it is very unlikely that a large release would be unignited. The total heat flux to the ignited pool, and hence the evaporation/burning rate, is 1.4–1.5 times that for the unignited pool. Some literature [16] suggests that the burning rate for an ignited pool is 2.5–3.5 times the evaporation rate of an unignited pool. This range may be higher because the heat flux from the water to the pool is being underestimated, i.e. the effect of turbulence is not accounted for.

8. Related recent work

In recent studies, ABS Consulting [17] and Sandia National Laboratories [18] have advocated the time-based material–energy balance approach used here. However, they did not present adequate information to implement the approach and for their own illustrative predictions simply selected a total heat flux or burn rate.

ABS suggested a heat flux from water to LNG of 37 kW/m^2 but tested the sensitivity to values of 25 and 100 kW/m^2, since they noticed that variation in reported values. ABS reported corresponding evaporation fluxes for unignited pools. Recalling that the correlations for quiescent film boiling predict a heat flux of ~28 kW/m^2, the ABS heat fluxes correspond to the following turbulence factors:

Heat flux (kW/m^2)	Evaporation flux (kg/s m^2)	Turbulence factor
25	0.049	0.9
37	0.072	1.3
100	0.20	3.6

Heat fluxes and evaporation fluxes used in ABS study.

Even the highest of these values does not reflect as much turbulence as the Esso tests suggest.

For ignited spills on water, ABS used a burn rate of 0.282 kg/s m^2, which is about twice the value for the largest test on land (Montoir). The China Lake tests showed up to a factor of four, with that factor increasing with fire size, and those tests had a spill plate that greatly reduced the water–LNG turbulence.

Sandia used a burn regression rate of 3×10^{-4} m/s but tested the sensitivity to a rate of 2×10^{-4} m/s. Using typical LNG properties, these correspond to the following burn rates and total heat fluxes:

Regression rate ($\times 10^{-4}$ m/s)	Burn rate (kg/s m^2)	Heat flux (kW/m^2)
2	0.092	61
3	0.138	92

Burn regression rates used in Sandia study.

The higher of the two values approaches that for the largest test on land (Montoir), but is far below the expected value for fires on water.

Several organizations are evidently using the time-based material–energy balance approach in their internal software. These include ioMosaic (SuperChems) [19], BakerRisk (SafeSite$_{3G}$^{TM}) [16], and Applied Science Associates (LNGMAP) [20]. Publications seem to indicate that these orga-

nizations are struggling with the same issues addressed here, i.e., realistically estimating the relevant heat transfer terms in view of the lack of appropriate experimental data.

9. Conclusion

The keys to realistic modeling of evaporation and burning of LNG pools are:

- Use time-varying release rates.
- Use physical properties of LNG, not methane.
- Use a time-step analysis that captures the time-varying release rates and the changes in properties resulting from composition changes as the LNG vaporizes or burns.
- Use parameters that reflect actual spill conditions, including turbulence between the water and LNG.

This work shows that it is possible to use a material and energy balance approach for LNG evaporation and burning, rather than empirical evaporation or burning rates. This more theoretical approach provides a better basis for extrapolating to conditions far from those of the tests conducted to-date. However, there is considerable uncertainty about how to scale up the heat transfer from the water and from the fire to the pool. Additional analysis of tests to-date and also larger-scale and/or more focused test data will enable more accurate modeling of LNG pools.

Acknowledgments

The author gratefully acknowledges the contributions of C.M. (Chris) Robinson and others at the Upstream Research Company to this work, and the willingness of ExxonMobil to release this report to others who may benefit from it.

Appendix A. Heat transfer analysis

A.1. Heat transfer correlations

For unignited pools, the heat flow from the air above the pool is given by:

$$Q_{\text{air}} = h_{\text{a}}\pi R_i^2(T_{\text{a}} - T_{\text{L}}) \tag{A.1}$$

where Q_{air} is the heat flow from air above pool (W, Btu/s), h_{a} the heat transfer coefficient between air and the pool (W/m^2 C, Btu/s ft^2 F), R_i the pool radius at time step i (m, ft), T_{a} the ambient air temperature (K, F) and T_{L} is the temperature of LNG pool (K, F).

The heat transfer coefficient is given by:

$$h_{\text{a}} = \frac{Nu\, k_{\text{a}}}{D_i} \tag{A.2}$$

where Nu is the Nusselt number, k_{a} the thermal conductivity of air at film conditions (W/m K, Btu/s F) and D_i is the pool diameter at time step $i = 2R_i$ (m, ft).

A standard correlation for heat transfer to horizontal surfaces [21] is:

$$Nu = 0.037 Re^{0.8} Pr^{1/3} \tag{A.3}$$

where Re is the Reynolds number $= D_i v_{\text{a}} \rho_{\text{a}}/\mu_{\text{a}}$, Pr the Prandtl number of air vapor at film conditions $= c_{\text{a}}\mu_{\text{a}}/k_{\text{a}}$, v_{a} the wind speed (m/s, ft/s), ρ_{a} the density of ambient air at film conditions (kg/m^3, lb/ft^3), μ_{a} the viscosity of ambient air at film conditions (kg/m s, lb/ft s) and c_{a} is the heat capacity of ambient air at film conditions (J/kg K, Btu/lb F).

For the properties, "film conditions" means the average of the ambient air temperature and the pool (liquid LNG) temperature.

The radiative heat flow from above the pool, due to solar radiation or the pool fire, is:

$$Q_{\text{rad}} = q_{\text{rad}}\pi R_i^2 \tag{A.4}$$

where q_{rad} is the radiative heat flux (W/m^2 or Btu/s ft^2).

The heat transfer coefficient between the water and LNG, i.e. h_{w} in Eq. (8), is based on either film boiling or transition boiling, as appropriate.

A.2. Heat transfer coefficient for film boiling

The heat transfer coefficient for film boiling [5] is:

$$h_{\text{f}} = \frac{Nu_{\text{f}} k_{\text{VF}}}{L_{\text{c}}} \tag{A.5}$$

where h_{f} is the heat transfer coefficient between water and LNG (W/m^2 K, Btu/s ft^2 F), Nu_{f} the Nusselt number for film boiling, k_{VF} the thermal conductivity of vapor at film temperature (W/m K, Btu/s ft F) (film temperature taken as average of LNG and water temperatures) and L_{c} is the critical length (m, ft).

The critical length is:

$$L_{\text{c}} = 2\pi\sqrt{\frac{\sigma g_{\text{c}}}{g(\rho_{\text{L}} - \rho_{\text{V}})}} \tag{A.6}$$

where σ is the interfacial tension between LNG liquid and vapor (N/m, lbf/ft), g_{c} the unit conversion constant = 1 kg m/N s^2 = 32.174 lb ft/lbf s^2, g the acceleration due to gravity (m/s^2, ft/s^2), ρ_{L} the density of LNG liquid (kg/m^3, lb/ft^3) and ρ_{V} is the density of LNG vapor (kg/m^3, lb/ft^3).

The Nusselt number is given by [5]:

$$\text{Laminar region}: \quad Ar < 10^8, \qquad Nu_{\text{f}} = 0.19(Ar\, Pr)^{1/3} f_1 \tag{A.7}$$

$$\text{Turbulent region}: \quad Ar \geq 108, \qquad Nu_{\text{f}} = 0.0086\sqrt{Ar}\, Pr^{1/3} f_2 \tag{A.8}$$

where

$$Ar = \text{Archimedes number} = (2\pi)^3 \frac{(\sigma g_{\text{c}})^{1.5}\rho_{\text{V}}}{\mu_{\text{V}}^2\sqrt{g(\rho_{\text{L}} - \rho_{\text{V}})}},$$

$$Pr = \text{Prandtl number of LNG vapor} = \frac{c_{\text{V}}\mu_{\text{V}}}{k_{\text{V}}} \tag{A.9}$$

The dimensionless functions f_1 and f_2 are given by [22]:

$$\text{Laminar region}: \quad \text{For } \frac{\Delta H_{\text{V}}}{c_{\text{L}}\,\Delta T} > 1.4,$$

$$f_1 = 0.89\left(\frac{\Delta H_V}{c_L\,\Delta T}\right)^{1/3}, \qquad \text{For } \frac{\Delta H_V}{c_L\,\Delta T} \le 1.4, \quad f_1 = 1 \tag{A.10}$$

$$\text{Turbulent region}: \quad \text{For } \frac{\Delta H_V}{c_L\,\Delta T} > 2,$$

$$f_2 = 0.71\sqrt{\frac{\Delta H_V}{c_L\,\Delta T}}, \qquad \text{For } \frac{\Delta H_V}{c_L\,\Delta T} \le 2, \quad f_2 = 1 \tag{A.11}$$

where ΔH_V is the heat of vaporization of LNG (J/kg, Btu/lb), c_L the heat capacity of LNG liquid (J/kg C, Btu/lb F) and ΔT is the temperature difference between water and LNG (K, °F).

The minimum temperature difference required for film boiling [5] is:

$$\Delta T_{min} = (T_{pc} - T)\left[0.16 + 2.4\left(\frac{\rho_L c_L k_L}{\rho_w c_w k_w}\right)^{1/4}\right] \tag{A.12}$$

where T_{pc} is the pseudo-critical temperature of LNG (K, F), T the temperature of LNG (K, F), ρ_L the density of LNG liquid (kg/m^3, lb/ft^3), k_L the thermal conductivity of LNG liquid (W/m K, Btu/s F), ρ_w the density of water (kg/m^3, lb/ft^3), c_w the Heat capacity of water (J/kg K, Btu/lb F) and k_w is the thermal conductivity of water (W/m K, Btu/s F).

Eq. (A.12) is based primarily on pure component data, and for pure components the critical temperature is used instead of T_{pc}. Limited data on binary mixtures indicates that mole fraction averaging of ΔT_{min} values works well. This is equivalent to using the pseudo-critical temperature, as shown in Eq. (A.12).

If the temperature difference between the water and LNG falls below ΔT_{min}, the boiling enters the transition regime. Simulations indicate that this occurs late in the vaporization process.

A.3. Heat transfer coefficient for transition boiling

The recommended procedure for estimating the heat transfer coefficient in the transition regime is to estimate the heat flux and then divide it by the temperature difference. The heat flux is estimated by a sort of interpolation, using the heat fluxes and temperature differences at the two points bounding the transition regime [5].

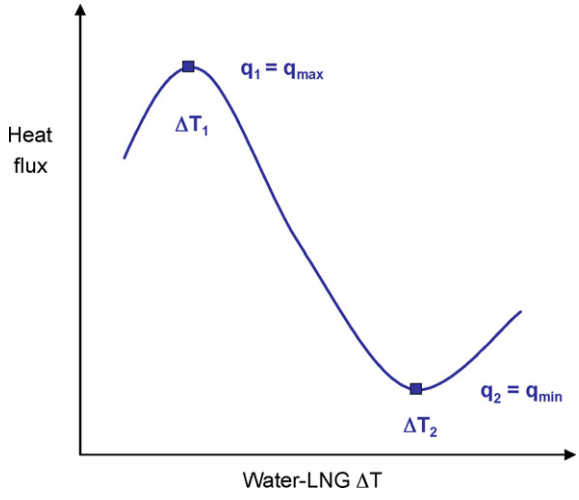

$$h_t = \frac{fq_1 + (1-f)q_2}{\Delta T} \tag{A.13}$$

$$f = \left[1 - \frac{\Delta T - \Delta T_1}{\Delta T_2 - \Delta T_1}\right]^7 \tag{A.14}$$

where h_t is the heat transfer coefficient between water and LNG (W/m^2 K, Btu/s ft^2 F), ΔT the temperature difference between water and LNG (K, °F), q_1 the heat flux at maximum flux point (W/m^2, Btu/s ft^2), q_2 the heat flux at minimum flux point (W/m^2, Btu/s ft^2), ΔT_1 the temperature difference at maximum flux point (K, °F), ΔT_2 the temperature difference at minimum flux point (K, °F) = ΔT_{min} (Eq. (A.13)) and f is the interpolation function.

The correlation for ΔT_1 is:

$$\Delta T_1 = 0.625[q_1\sigma T]^{1/3}\frac{\left[10/\left(\sqrt{\rho_w c_w k_w}\right) + \sqrt{\mu_L/\rho_L}/k_L\right]^{2/3}}{\left[1 + 10\sqrt{\rho_L c_L k_L/\rho_w c_w k_w}\right]^{1/3}} \frac{}{1 + 10(\rho_{VF}/(\rho_L - \rho_{VF}))^{2/3}} \tag{A.15}$$

where ρ_{VF} is the density of the LNG vapor at the film temperature (taken as the average of the LNG and water temperatures). If field units are used in this equation, the interfacial tension σ in lbf/ft must be divided by 778.169 ft lbf/Btu to obtain Btu/ft^2.

For LNG on water, ΔT_1 typically varies from ~3 to 4 K (5–7 °F), and ΔT_2 varies from ~140 to 190 K (250–340 °F) as vaporization proceeds. Hence, f is very small, and vaporization moves only slightly into the transition region. The heat transfer coefficient increases as a result of the transition.

Two correlations for q_1 are [23]:

$$q_1 = 0.168\,\Delta H_v\sqrt{\rho_V}[\sigma g_c(\rho_L - \rho_V)]^{1/4} \tag{A.16}$$

and

$$q_1 = \frac{0.18\,\Delta H_V \rho_V [\sigma g_c(\rho_L - \rho_V)]^{1/4}}{1 + 2\sqrt{\rho_V/\rho_L} + (\rho_V/\rho_L)}\sqrt{\frac{\rho_L - \rho_V}{\rho_L \rho_V}} \tag{A.17}$$

In this work, the minimum of these two values of q_1 was used.

Although there are several correlations for q_2, in order to avoid a discontinuity in the heat transfer coefficient as the transition region is entered, it is best to take q_2 as the heat flux at the last time step for which vaporization was in the film boiling regime ($\Delta T < \Delta T_{min}$).

A.4. Comparison with other correlations

For validation, predictions of the above correlation for the film boiling heat transfer coefficient were compared with those from another correlation [24] and found to agree reasonably well. Predictions of the minimum temperature difference required for film boiling were validated by using a correlation for the minimum heat flux for film boiling [24] and dividing that heat flux by the film boiling heat transfer coefficient to obtain the corresponding minimum temperature difference. Again, the two approaches agreed reasonably well.

A.5. Effect of fluid velocity on heat transfer coefficient

A standard correlation for heat transfer from a fluid to a cylinder [25] was applied to flow of seawater at a typical ambient temperature. A cylinder is a reasonable approximation of the column of LNG entering the seawater from a hole in a tank on a ship. The heat transfer coefficient is proportional to the fluid velocity to a power that depends on the diameter of the cylinder as follows:

$$\frac{h}{h_0} = \left(\frac{v}{v_0}\right)^n \tag{A.18}$$

where h is the heat transfer coefficient between seawater and LNG at velocity v and h_0 is the heat transfer coefficient at reference velocity v_0:

$$n = 0.0512 \ln D + 0.8723 \tag{A.19}$$

where D is the diameter of cylinder [= hole diameter] (m). This relationship is shown in the following figure.

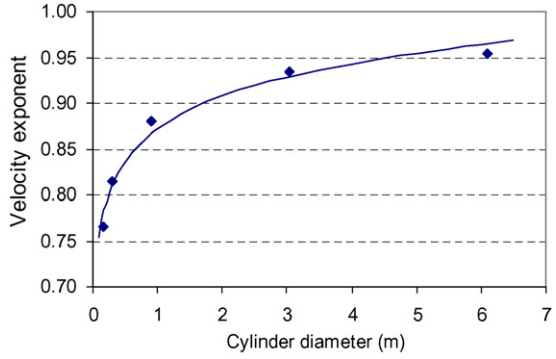

Relationship of Velocity Exponent to Cylinder Diameter

This relationship can be used for the effect of fluid velocity on the LNG–water turbulence factor.

References

[1] F. Briscoe, P. Shaw, Spread and evaporation of liquid, Prog. Energy Combust. Sci. 6 (1980) 127–140.
[2] W.G. May, W. McQueen, R.H. Whipp, Spills of LNG on water, AGA 1973 Operating Section Proceedings, Paper 73-D-9, 1973, p. D-143.
[3] T.A. Cavanaugh, J.H. Siegell, K.W. Steinberg, Simulation of vapor emissions from liquid spills, J. Hazard. Mater. 38 (1994) 41–63.
[4] L. Post, HGSYSTEM 3.0, Technical Reference Manual, TNER.94.059, Shell Research Ltd., 1994.
[5] C. Conrado, V. Vesovik, The influence of chemical composition on vaporisation of LNG and LPG on unconfined water surfaces, Chem. Eng. Sci. 55 (2000) 4549–4562.
[6] R. Boe, Pool boiling of hydrocarbon mixtures on water, Int. J. Heat Mass Transfer 41 (1998) 1003–1011.
[7] J. Dahlsveen, R. Kristofferson, L. Saetran, Jet mixing of cryogen and water, turbulence and shear flow phenomena, in: Proceedings of the Second International Symposium, vol. 2, Stockholm, Sweden, 2001, pp. 329–334.
[8] D. Burgess, J. Biordi, J. Murphy, Hazards of spillage of LNG into water, PMSRC Report 4177, MIPR no. Z-70099-9-12395, 1972.
[9] D.S. Burgess, J.N. Murphy, M.G. Zabetakis, Hazards associated with the spillage of liquefied natural gas on water, RI-7748, U.S. Dept. of Interior, 1970.
[10] D.R. Jenkins, A.C. Timmers, LNG plant safety in the light of recent experimental trials and theories, in: Proceedings of the Seventh International Conference on Liquefied Natural Gas, Jakarta, Indonesia, 1983, p. 6.
[11] P.J. Rew, W.G. Hulbert, Development of pool fire thermal radiation model, HSE Contract Research Report 96/1996, W.S. Atkins, 1996, p. 7.
[12] Gas Research Institute, LNGFIRE3: a thermal radiation model for LNG fires, GRI-89/0176, PB91-220137, 1980.
[13] M.J. Pritchard, T.M. Binding, FIRE2: a new approach for predicting thermal radiation levels from hydrocarbon pool fires, I. Chem. E. Sympos. Ser. 130 (1992) 491–505.
[14] R.M. Pitblado, J. Baik, G. Hughes, C. Ferro, S.J. Shaw, Consequences of LNG marine incidents, in: Proceedings of the CCPS Conference, Orlando, FL, June 29–July 1, 2004.
[15] A.L. Schneider, Liquefied natural gas spills on water: fire modeling, J. Fire Flammability 11 (1980) 302.
[16] J. Woodward, Modeling dynamic aspects of LNG spill, The BakerRisk Bulletin 10, issue 1, 2005.
[17] ABS Consulting, Consequence assessment methods for incidents involving releases from liquefied natural gas carriers, Report GEMS 1288209, Federal Energy Regulatory Commission, Contract FERC04C40196, 2004.
[18] Sandia National Laboratories, Guidance on risk analysis and safety implications of a large liquefied natural gas (LNG) spill over water, SAND2004-6258, 2004.
[19] S.R. Saraf, G.A. Melham, Modeling LNG pool spreading and vaporization, in: Proceedings of the AIChE Meeting, Atlanta, GA, April 10–14, 2005.
[20] N. Whittier, C. Swanson, K. Jayko, LNGMAP: a state-of-the-art LNG release, transport and fate model system for marine spills, in: Proceedings of the Conference LNG: The Environmental and Safety Agenda, AIChE and CSChE, September, 2005.
[21] F.P. Incropera, D.P. DeWitt, Fundamentals of Heat and Mass Transfer, 5th ed., Wiley, Hoboken, NJ, 2002, p. 397.
[22] V.V. Klimenko, Film boiling on a horizontal plate—new correlation, Int. J. Heat Mass Transfer 24 (1981) 69–79.
[23] P.J. Waite, R.J. Whitehouse, E.B. Winn, The spread and vaporization of cryogenic liquids on water, J. Hazard. Mater. 8 (1983) 165–184.
[24] F.P. Incropera, D.P. DeWitt, Fundamentals of Heat and Mass Transfer, 5th ed., Wiley, Hoboken, NJ, 2002, p. 604.
[25] F.P. Incropera, D.P. DeWitt, Fundamentals of Heat and Mass Transfer, 5th ed., Wiley, Hoboken, NJ, 2002, p. 411.